

Assessing mechanical properties of single-layer B-doped C_3N and N-doped BC_3 nanosheets and their hybrid

Fatemeh Molaie,¹ Kasra Einalipour Eshkalak,² Sadegh Sadeghzadeh,^{3*} Hossein Siavoshi⁴

1- Ph.D. student, Mining and Geological Engineering Department, The University of Arizona, Arizona, USA

2- Facilities and Piping Department, Qazvin Tarom Copper Company and MSc of Nanotechnology Engineering, School of Advanced technologies, Iran University of Science and Technology, Tehran, Iran

3,*- Associate Professor of Nanotechnology Engineering, School of Advanced Technologies, Iran University of Science and Technology, Tehran, Iran, sadeghzadeh@iust.ac.ir.

4- Graduate student, Mining and Geological Engineering Department, The University of Arizona, Arizona, USA

Abstract

In this study, we analyzed the mechanical properties of single-layers C_3N doped with boron (B) atoms and BC_3 doped with nitrogen (N) atoms, as well as hybrid C_3N - BC_3 nanosheets intraplate by forming covalent bonds using molecular dynamics simulation. The results show that the monolayer of C_3N has higher mechanical properties than common materials, but adding B atoms and a single-layer of BC_3 to it causes irreparable mechanical damage. However, the BC_3 sheets did not react similarly and the mechanical properties were not significantly reduced by adding nitrogen atoms and the C_3N to it; in some cases, the mechanical properties of the structure did not increase. Therefore, by adding 5% of boron atom to the C_3N structure in the armchair direction, Young's modulus, failure stress, and strain were reduced by 6, 19, and 20 percent, respectively. When we added a nitrogen atom to the BC_3 structure, failure stress and strain reduced by 1.5 and 2 percent, respectively, but Young's modulus increased by 1%. One of the reasons for such behaviors is stronger binding energy between N-C atoms compared to B-C. Consequently, these weak bonds cause BC_3 failure in hybrid systems. The results provide a fundamental understanding of the design of hybrid structures used in the nanodevices based on advanced 2D materials.

Keywords: C_3N and BC_3 doped nanosheets; C_3N - BC_3 hybrid; Mechanical properties; Molecular dynamics

1 Introduction

In recent years, 2D materials have attracted the attention of many researchers and scientists due to their unique features and potential applications in nano-electronic and nano-electromechanical devices [1]. Graphene monolayer is one of the most prominent of these materials, which was accidentally synthesized in 2004 using mechanical exfoliation [3,2]. Regardless of its remarkable properties, it has been associated with problems such as zero band-gap and the inability to absorb sodium, lithium, and other metallic atoms. Researchers have offered approaches to solve these challenges. For example, hybridizing graphene with other 2D materials, creating controlled holes to open up the band-gap in the graphene structure, and doping atoms such as nitrogen and boron in graphene. These approaches could solve the problem of absorbing different atoms on the surface of graphene and show the conversion of graphene to strong catalysts. However, each of these approaches have been challenging and demonstrate more interesting performance features [4-10]. Due to the strong structural similarity of graphitic structures such as C_3N [11] and BC_3 [12], some of these problems have been solved as an anode [14,13] and have been commonly used in many applications (e.g. lithium batteries). The results demonstrate that C_3N and BC_3 are semiconductor with a band-gap of 0.39eV and 0.54eV, respectively [15,11]. Therefore, they are expected to be suitable alternatives to graphene or hybrids to open the band-gap and build field-effect transistors based on graphene.

Recently, some theoretical proposals for nano-electronic products, catalysts, magnetic applications, energy storage, and photocatalysts have been made for BC_3 nanoparticles as an advantageous structure [16-18]. Reports are available of doping of various atoms in these two structures to alter the chemical, electronic, and magnetic properties [19-22]. In 2013, Beheshtian et al. studied the doping of aluminum (Al) and silicon (Si) atoms in a single layer of BC_3 . Their results show that the doping of these atoms makes the single layer more reactive and sensitive than the H_2CO molecule. However, the doping of the Si atom is a better strategy for making chemical sensors due to the shorter recovery time and higher sensitivity of the Si-doped sheet [23]. Using the first-principles calculations, Yang et al. (2012) examined high-capacity hydrogen storage on the Li-doped BC_3 sheet. The Li atoms can be strongly absorbed on the BC_3 structure without clustering: each Li atom absorbed on the BC_3 supercell can absorb four hydrogen molecules [24]. Recently, Bingling et al. introduced a boron-doped C_3N monolayer as a promising metal-free oxygen reduction reaction catalyst by using the first-principle calculations. Their results suggest that the formation of the B-doped C_3N monolayer is highly exothermic, and the replacement of the B atom with carbon shows a lower catalytic

activity than the replacement with the N atom for the oxygen reduction reaction [25]. On the other hand, hybrids of 2D materials have been studied by many researchers because of the appearance of new properties and their use in some applications [26]. Extensive studies have been reported on the mechanical properties of 2D structures doped with different atoms and hybrids of them [27-31]. Using molecular dynamics simulation, Mortazavi et al. (2012), investigated the mechanical properties of N-doped graphene, and showed that the ultimate strength and Young's modulus of graphene with a concentration of 6% nitrogen atom respectively decreased and increased [32]. Furthermore, the molecular dynamics research of the effect of B-doped graphene on the mechanical and thermal properties was studied. The results showed that by replacing the boron atoms with carbon atoms in graphene, Young's modulus and tensile strength decreased, while the reduction of tensile strength was more significant. On the other hand, it was observed that with only 0.75% concentration of boron atoms in graphene, the thermal conductivity decreased by 60% and led to a vanishing chirality effect [33]. The mechanical properties of pure BC_3 and C_3N have been studied and details of the results are available under different conditions [35, 34, 18].

In a study of molecular dynamics, the mechanical properties of C_3N perfect sheets and those with defects, such as cracks and cavities, were examined [36]. The crack length and diameter of the various holes have been studied and predicted at different temperatures for mechanical properties. Results show that cracks and cavities reduce the strength of nanosheets; moreover, increasing the temperature is a weakening effect on tensile strength. As the temperature rises from 200 to 900 Kelvin, Young's modulus decreases by 9% [36]. In 2019, using a simulation of molecular dynamics, Zahedi et al. studied the mechanical properties of BC_3 with a focus on the effect of defects at different temperatures. The results show that the mechanical properties of BC_3 , such as C_3N are decreased, and the temperature increases due to defects. The results of that work are compared with C_3N and demonstrate that the mechanical properties of C_3N under the same conditions are higher than BC_3 . Moreover, the values of elastic modulus are higher due to the role of stiffening in C-N bond compared with C-B bond ones [37]. The mechanical properties of the hybrid of 2D materials are available using the simulation of molecular dynamics [39, 38, 6]. Using the molecular dynamics simulation technique, in 2013, Zhao et al. examined the mechanical properties of a hybrid graphene and hexagonal boron-nitride (h-BN) sheet with the concentration of BN ranging from 0% to 100%. Irrespective of the form and distribution of BN, the Young's modulus of the hybrid sheet decreases with increasing concentration of BN. However, adding a small amount of BN to graphene causes a noticeable drop in the strength of the hybrid sheet.

There have been no reports of the mechanical properties of BC₃ and C₃N doped with different atoms and hybrid C₃N-BC₃ structures. Due to the unique properties of these two structures, their potential applications in various industries, their structural similarity with graphene, and their ability to replace graphene in some electronic devices due to the weakness of graphene, more detailed studies of the mechanical properties of these types of graphene-like structures are important. Therefore, we use a molecular dynamics simulation technique to examine the mechanical properties of C₃N and BC₃, doped with both boron and nitrogen atoms. The effects of nitrogen and boron concentration on the mechanical and elastic properties of the two structures have been studied and compared in different conditions. The findings indicate that the outstanding mechanical properties of BC₃ and C₃N make them promising designers, and introduce them as new catalysts to design new nanoelectronics and nanoelectromechanical devices.

2 Computational Methods

All simulations in this study were done with the help of a large-scale atomic/molecular mass parallel simulator (LAMMPS) software package [40]. Image processing and analysis were completed by the OVITO visualization software [41]. The interaction between carbon-nitrogen atoms in C₃N and carbon-boron in BC₃ have been presented by Kinaci et al. [43 ,42]. However, to investigate the mechanical properties of these two structures, the optimized potential of interatomic bonds has been used in previous reports [37 ,35]. In this potential, the relationship between the energy and the displacement of atoms with respect to each other is expressed as:

$$U_{ij} = f_c(r_{ij})[f_R(r_{ij}) + b_{ij}f_A(r_{ij})] \quad (1)$$

Function $f_R(r_{ij})$ indicates the repulsion potential of two particles (e.g., in a nucleus-nucleus interaction) and $f_A(r_{ij})$ denotes the attraction potential resulting from valence electrons. b_{ij} is a bonding strength term, which depends on the local atomic medium surrounding a specific bond. It is a decreasing function of atoms rearrangement number. b_{ij} contains all the multi-particle effects of potential. These relations express existing functions in these potentials:

$$f_R(r_{ij}) = -A_{ij} e^{-\lambda_{ij}r_{ij}}, \quad f_A(r_{ij}) = -B_{ij} e^{-\mu_{ij}r_{ij}} \quad (2)$$

$$f_c(r_{ij}) = \begin{cases} 1 & r_{ij} < R_{ij} \\ \frac{1}{2} + \frac{1}{2} \cos \left[\frac{\pi(r_{ij} - R_{ij})}{S_{ij} - R_{ij}} \right] & R_{ij} \leq r_{ij} \leq S_{ij} \\ 0 & r_{ij} < S_{ij} \end{cases} \quad (3)$$

The required constants are defined as follows:

$$b_{ij} = X_{ij}(1 + B_i^{n_i} \xi_{ij}^{n_i})^{-0.5n_i}, \xi_{ij} = \sum_{k \neq i,j} f_c(r_{ik}) \omega_{ik} g(\theta_{ijk}), g(\theta_{ijk}) = 1 + \frac{c_i^2}{d_i^2} - \frac{c_i^2}{d_i^2 + (h_i + \cos \theta_{ijk})^2}, \omega_{ik} = e^{\left[\mu_{ik}^3 (r_{ij} - r_{ik})^3 \right]}, \lambda_{ij} = \frac{(\lambda_i + \lambda_j)}{2}, \mu_{ij} = \frac{(\mu_i + \mu_j)}{2}, A_{ij} = \sqrt{A_i A_j} \text{ } \text{ } B_{ij} = \sqrt{B_i B_j}, R_{ij} = \sqrt{R_i R_j}, S_{ij} = \sqrt{S_i S_j} \quad (4)$$

Indices i, j and k specify the existing atoms in the ijk bond. rij and rik indicate the lengths of ij and ik bonds, respectively, with θ_{ijk} being the angle between them. These coefficients have been used with regard to the coefficients presented above.

This project considers the dimensions of the structures $20 \times 20 \text{ nm}^2$. The total number of atoms present in the simulation is 16,044; the share of carbon atoms is 12,012; and the total share of boron and nitrogen atoms in BC_3 and C_3N structures is 4032 (Figure 1). Simulation in a state of equilibrium and system was subjected to tensile load with a strain rate of 10^8 s^{-1} that tensile in the X and Y direction are armchair (AC) and zigzag (ZZ), respectively. In all the cases, the Nose-Hoover algorithm at a constant temperature (300 K) and pressure (NPT) with time step 0.25 fs for 50 ps were used to equilibrate the system, and the velocity Verlet algorithm was used to integrate the Hamiltonian equations of the determined motion. The boundary conditions are periodic along the in-plane directions.

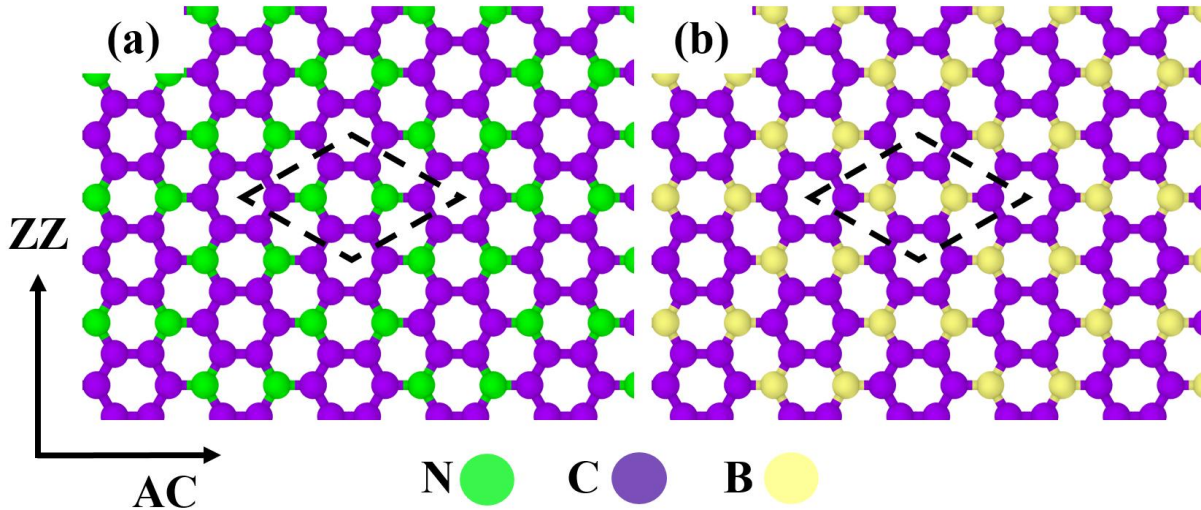


Figure 1. The C_3N (a) and BC_3 (b) atomic configuration with a honeycomb structure includes carbon-nitrogen and carbon-boron atoms, respectively. In their ideal structures, each boron and nitrogen atom is surrounded by three carbon atoms. In both structures, the unit cell with broken lines is visible. Carbon, nitrogen and boron atoms are presented in purple, green, and yellow, respectively.

The virial stress resulting from the tensile load was computed according to Eq. 6.

$$\sigma_{\alpha\beta} = \frac{1}{V} \left(\sum_{i=1}^N m v_{\alpha}^i v_{\beta}^i + \frac{1}{2} \sum_{l=1}^{N-1} \sum_{j=i+1}^N r_{ij,\alpha}^{N-1} F_{ij,\beta} \right) \quad (5)$$

In the above equation, V is the total volume of a simulated nanosheet, α and β are the indices of the Cartesian coordinate system, and m and v_{α}^i are the mass and the velocity of component α in atom i , respectively. Furthermore, $r_{ij,\alpha}$ and $F_{ij,\beta}$ indicate the separation distance and separation force of components α and β , between atoms i and j , respectively. The volumes of C_3N and BC_3 sheets were obtained by assuming a thickness of 3.2\AA for C_3N [35] and 3.3\AA for BC_3 [37]. After the calculation of stress tensor on each individual atom, the equivalent stress of a sheet was calculated based on von Mises stress to better understand how to stress distribution in the present work structures, as illustrated in the following equation

$$\sigma_{V-M} = \sqrt{\frac{1}{2} [(\sigma_{11} - \sigma_{22}) + (\sigma_{11} - \sigma_{33}) + (\sigma_{22} - \sigma_{33}) + 6(\sigma_{12}^2 + \sigma_{23}^2 + \sigma_{31}^2)]} \quad (6)$$

Where $\sigma_{1,2,3}$ represents the stress in three directions x , y and z .

3 Results and discussion

3.1 Validation

To estimate the accuracy of the simulations, the results of mechanical testing and the stress-strain diagram of single layers C_3N and BC_3 in the direction of ZZ were compared with works by Shirazi and Zahedi under the same conditions. Figure 2 is a suitable guarantor ensuring the correctness of the simulations. In addition, the mechanical properties of C_3N were higher than BC_3 . Nonetheless, in different applications, this difference can vary.

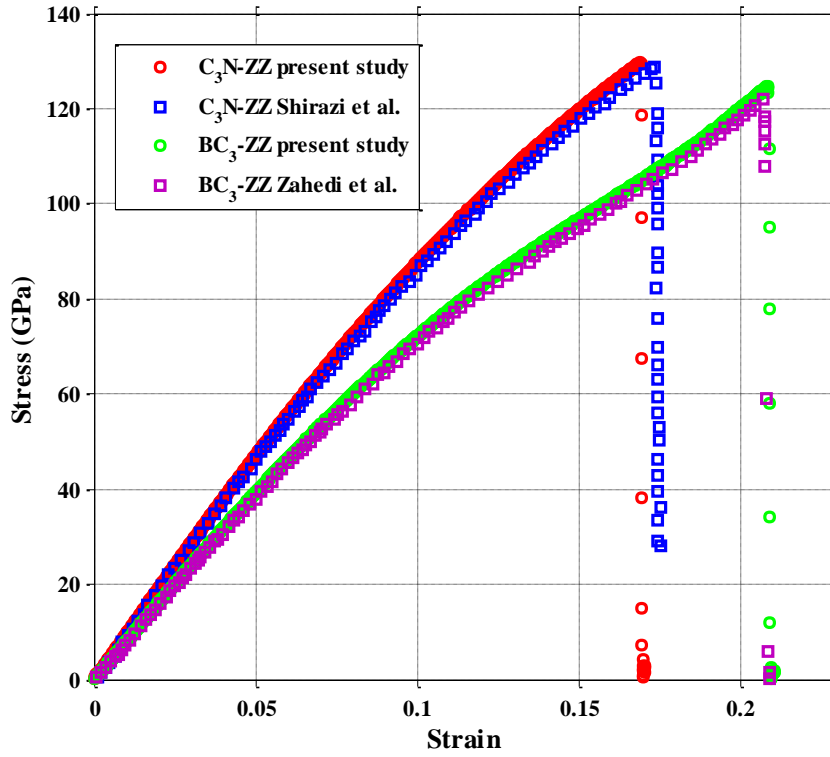


Figure 2. Comparison of C_3N and BC_3 stress-strain graphs with the results of Shirazi and Zahedi et al. works. The red and green circles are the results of this study, and the blue and purple squares are the results of previous works [36, 37].

Hereafter, for all mechanical tests, a strain rate of $10^9 s^{-1}$ was used to reduce simulation time. Previous studies have shown that the strain rate parameter has significant effects on mechanical properties, so when the strain rate increases, the mechanical properties increase as well [44]. Considering the average strain rate of the previous works, the stress and strain curves of the desired systems have been reported in this work. From this point forward, the dimensions of the studied structures are considered $6 \times 6 \text{ nm}^2$.

3.2 Mechanical properties of N-doped BC_3 and B-doped C_3N sheets

The entrance of specific impurities into semiconductors can alter their electrical, chemical, and even mechanical properties. Doping is the primary process used in the microelectronics industry to make significant components such as diodes and transistors. In nanotechnology, doping has other uses, including forming piezoresistors for mechanical converters or creating etch stop-layers. In this section, the doping effects of B and N atoms in C_3N and BC_3 are investigated due to the high consumption of boron and nitrogen atoms in different semiconductors and the emergence of new properties, discussed in detail in the introduction. In the following section, we used the potential of Tersoff modified by Zhang et al. [45] for the emergence of BNC two-dimensional structures in the studied systems. We studied

the mechanical properties in both AC and ZZ directions by atomic doping in structures and the formation of covalent bonds. The weight percentages of added atoms were considered to be 1 to 5 percent and were compared. Often, the atom is doped in two separate ways, such that the doped atom is replaced only by the carbon atom in the structures, and then the doped atom is considered randomly instead of both the carbon and nitrogen atoms in C_3N and carbon and boron in BC_3 .

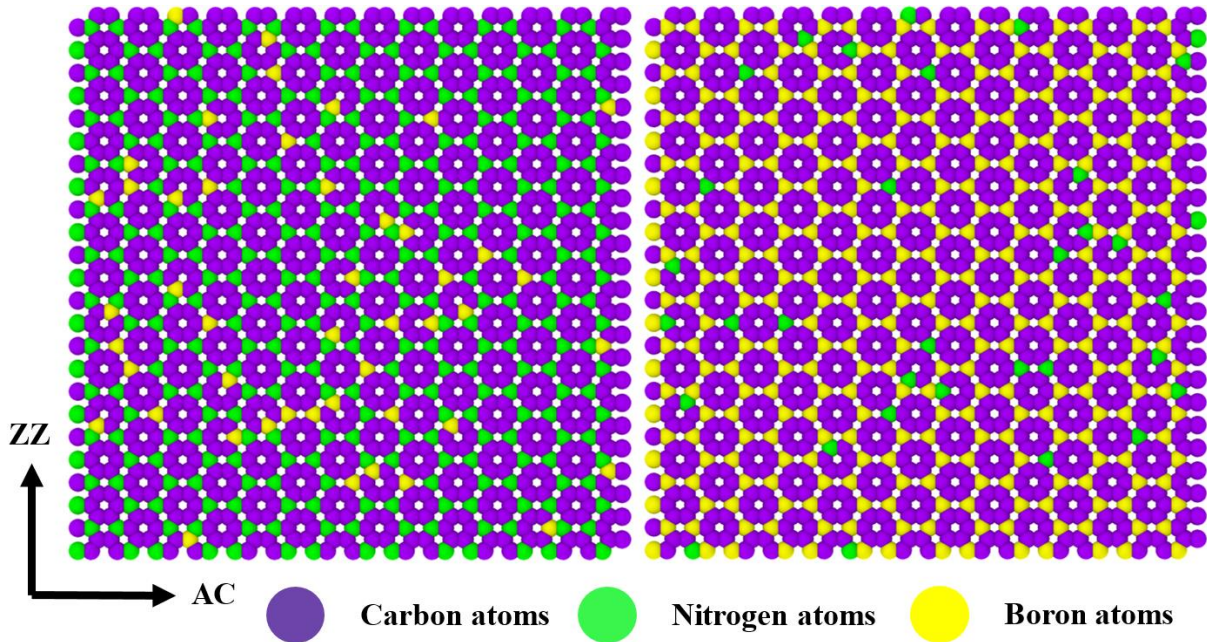


Figure 3. MD model of Boron-doped C_3N (left panel) and Nitrogen-doped BC_3 (right panel) sheets with three wt. % in concentration.

Figure 4 Figures 3 and 4 show the stress-strain curves under different conditions for C_3N and BC_3 , respectively. Accurate and comparable results of Young's modulus, stress, and strain failure are listed in Table 1. The highest and lowest results for atomic doping in different conditions are represented by green and red highlights. The results show that by adding B atoms to the structure of C_3N , the mechanical properties were greatly reduced; however, when the N atom was doped in BC_3 , the mechanical properties did not significantly reduce, and in some cases, even improved. Young's modulus is more than the failure of stress and strain. Various mechanisms can be envisioned to increase mechanical properties. The increase in Young's modulus can be attributed to the higher bond energy between N-C compared to B-C. Another reason could be the removal of the stress concentration from the structure. Consequently, atom B may create a higher stress concentration in the BC_3 structure around it. Removing and replacing it with nitrogen atom eliminates this concentrated stress and changes the failure mechanism. Adding a nitrogen atom to the structure does not necessarily reduce the mechanical

properties. The mechanical properties increase during the emergence of new properties under ideal conditions.

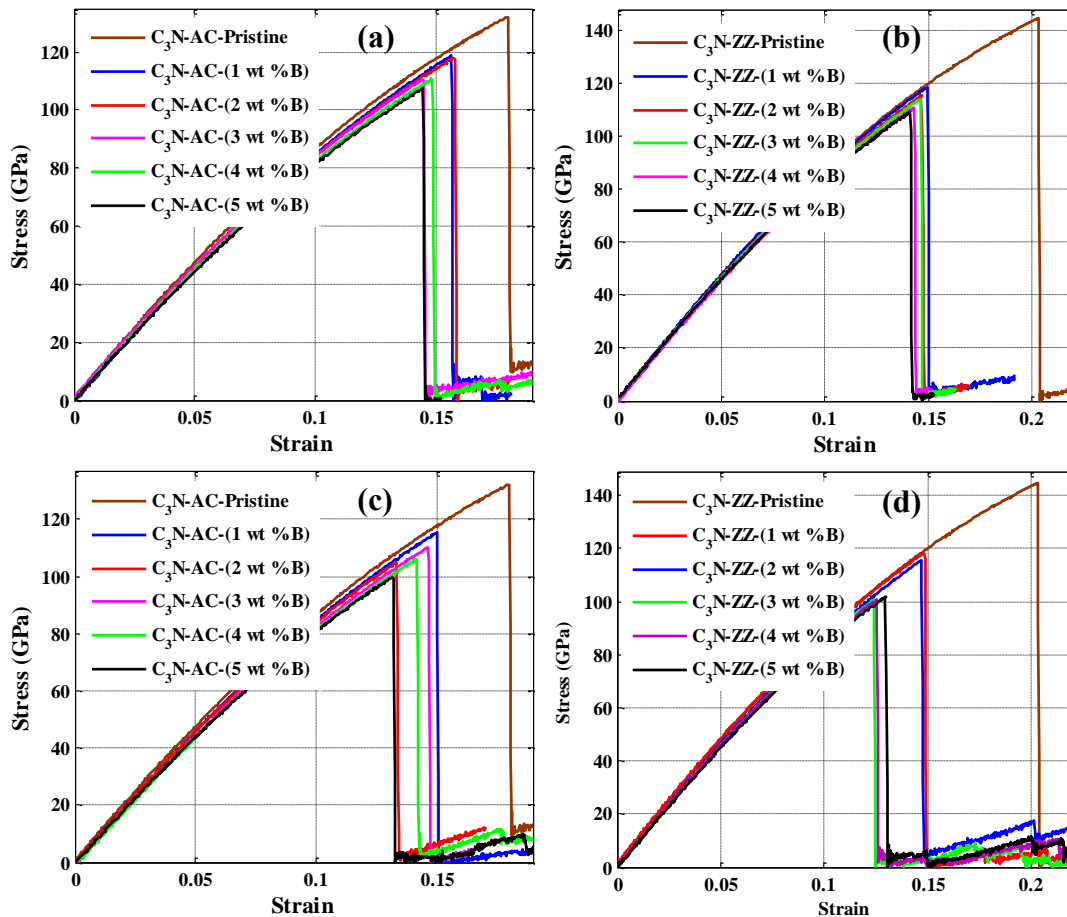


Figure 4. Stress-strain curve of B-doped C_3N sheet in an armchair (a, c) and zigzag (b, d) directions, determined by empirical MD simulation with different weight percentages. a, b: C_3N -Boron doped instead carbon. c, d: C_3N -Boron doped instead of carbon and nitrogen.

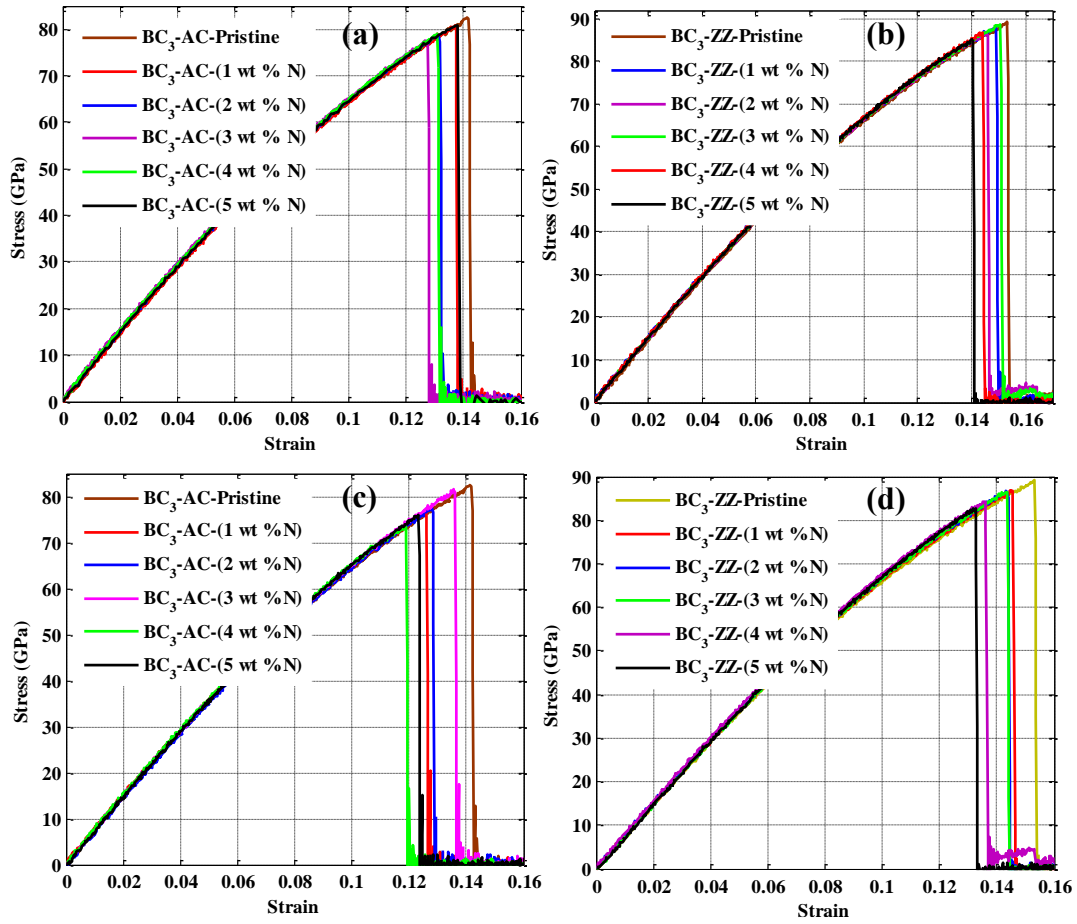


Figure 5. Stress-strain curve of N-doped BC_3 sheet in an armchair (a, c) and zigzag (b, d) directions, determined by empirical MD simulation with different weight percentages. a, b: C_3N -Boron doped instead carbon. c, d: C_3N -Boron doped instead of carbon and nitrogen.

Table 1. Comparison of Young's modulus, failure strength, and strain of C_3N -B doped and BC_3 -N doped in the different weight percentages and modes using molecular dynamics simulations.

Structure	Failure strength (GPa)				Failure Strain (%)				Young's modulus (GPa)				
	Value (GPa)		Variation (%)		Value (%)		Variation (%)		Value (GPa)		Variation (%)		
	AC	ZZ	AC	ZZ	AC	ZZ	AC	ZZ	AC	ZZ	AC	ZZ	
C_3N-B doped instead C (wt. %B)	0	132	144	-	-	17.9	20.3	-	-	959	957	-	-
	1	119	118	-10	-18	15.6	14.9	-13	-27	949	957	-1	0
	2	118	115	-11	-20	15.7	14.7	-12	-28	932	933	-3	-3
	3	111	114	-16	-21	14.4	14.6	-20	-28	929	937	-3	-2
	4	111	111	-16	-23	14.8	14.3	-17	-30	922	937	-4	-2
	5	107	109	-19	-24	14.4	14.1	-20	-31	903	916	-6	-4
0	132	144	-	-	17.9	20.3	-	-	959	957	-	-	

C₃N-B doped instead C&N (wt. %B)	1	115	118	-13	-18	15	14.8	-16	-27	957	940	-0.2	-1.7
	2	105	116	-20	-19	13.3	14.7	-26	-28	929	946	-3	-1.1
	3	110	101	-17	-30	14.6	12.3	-18	-39	899	930	-6.2	-2.8
	4	106	101	-20	-30	14.1	12.5	-21	-38	891	927	-7	-3.1
	5	99	102	-25	-29	13.2	12.9	-26	-36	903	901	-5.8	-5.8
BC₃-N doped instead C (wt. %N)	0	83	89	-	-	14.1	15.3	-	-	721	718	-	-
	1	81	88	-1.6	-1.2	13.7	14.9	-2.8	-2.6	719	725	-0.2	+1
	2	79	87	-4.3	-2.8	13.1	14.5	-7	-5.2	726	745	+0.6	+3.7
	3	78	89	-5.5	-0.3	12.7	15	-10	-1.9	734	727	+1.8	+1.2
	4	79	87	-4	-2.7	13.1	14.4	-7	-5.8	679	750	-5.8	+4.4
	5	81	85	-1.5	-4.3	13.8	14	-2	-8.5	723	721	+0.2	+0.4
BC₃-N doped instead C&B (wt. %N)	0	83	89	-	-	14.1	15.3	-	-	721	718	-	-
	1	77	87	-6.6	-2.5	12.6	14.5	-11	-5.2	714	739	-1	+3
	2	78	87	-6	-2.8	12.8	14.3	-9.2	-6.5	727	750	+1	+4.4
	3	82	87	-1	-2.8	13.5	14.2	-4.2	-7.1	712	730	-1.2	+1.6
	4	74	84	-11	-5.5	11.8	13.6	-16	-11	726	755	+0.7	+5.1
	5	76	83	-8.4	-7	12.3	13.2	-13	-14	734	736	+2	+2.5

3.3 Mechanical properties of the hybrid C₃N–BC₃ sheet

In recent years, due to the emergence of new physical and chemical properties, several experimental and theoretical studies in the hybrid of two-dimensional materials with different configurations have been reported [46 ,38]. Therefore, we investigated the mechanical properties of hybrid C₃N-BC₃ sheets with different weight percentages (1.6, 5.4, 9.9, 21.4 and 45.6%, respectively). The configurations considered in this study are shown in Figure 6. Our hybrid structures are inside the plate to place a circular BC₃ within the C₃N. We examined the effect on mechanical properties of increasing the weight percentage. Figure 7 shows the stress-strain curves of all the different states in this study. Fracture stress and strain, as well as Young's modulus, decreased significantly with increasing BC₃ concentration embedded in C₃N in both AC (Fig. 7 a) and ZZ (Fig. 7 b) directions. The results show that by increasing this

concentration, the mechanical behavior of the system moves towards BC_3 sheets, and finally, the mechanical properties of BC_3 2D nanosheet are revealed. However, when C_3N was embedded in BC_3 , the mechanical parameters, including failure stress and strain, did not decrease significantly and for some cases increase with increasing concentration for both AC (Fig. 7 c) and ZZ (Fig. 7 d) directions. In general, the Young's modulus also increased at this stage. Changes in failure stress and strain, as well as Young's modulus, can be seen in Figure 8 for various configurations. The increase of C_3N concentration within BC_3 did not follow a particular order, but in general, the Young's modulus increased, and if the concentration increased, the system moved toward improving the mechanical properties. The exact values and the percentage of mechanical parameters fluctuation in this section are clearly shown in Table 2.

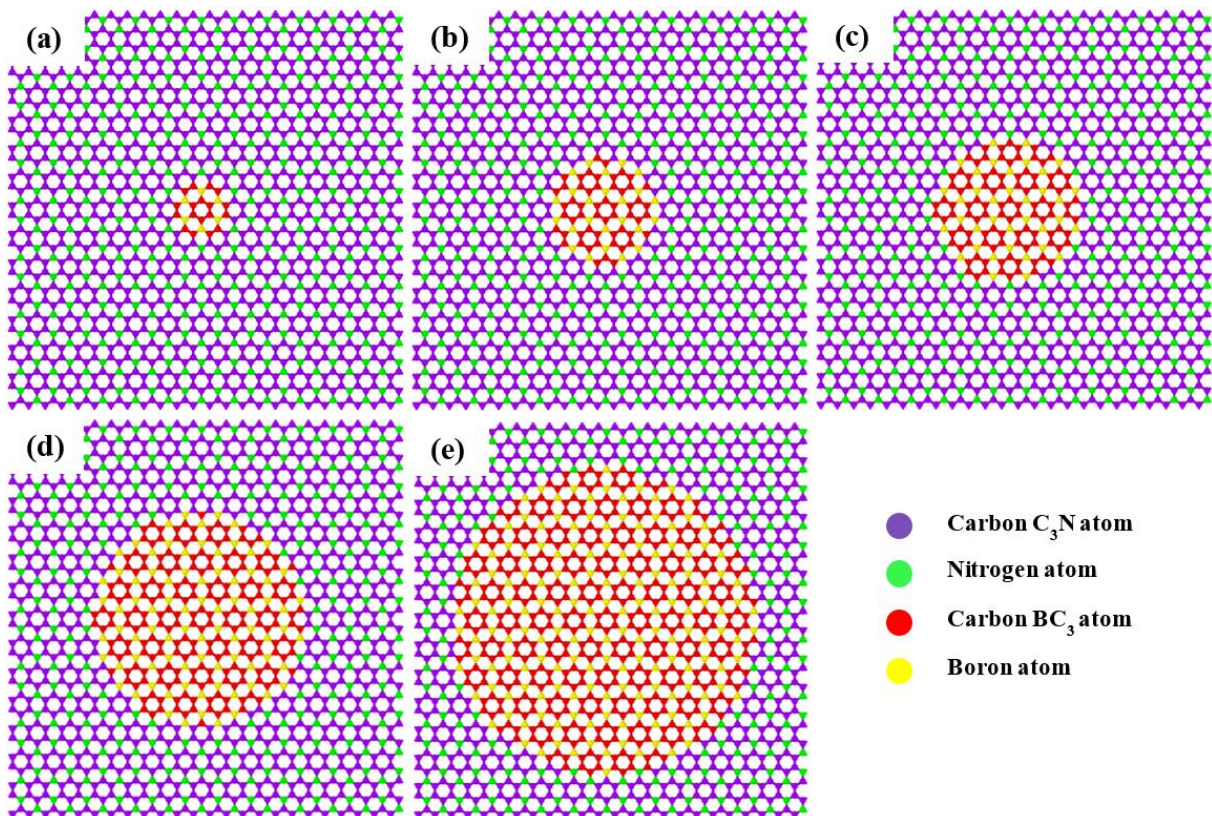


Figure 6. Different configurations of the hybrid C_3N-BC_3 sheet in this study to calculate the mechanical properties. The concentrations of BC_3 atoms are (a) 1.6%, (b) 5.4%, (c) 9.9%, (d) 21.4% and (e) 45.6%.

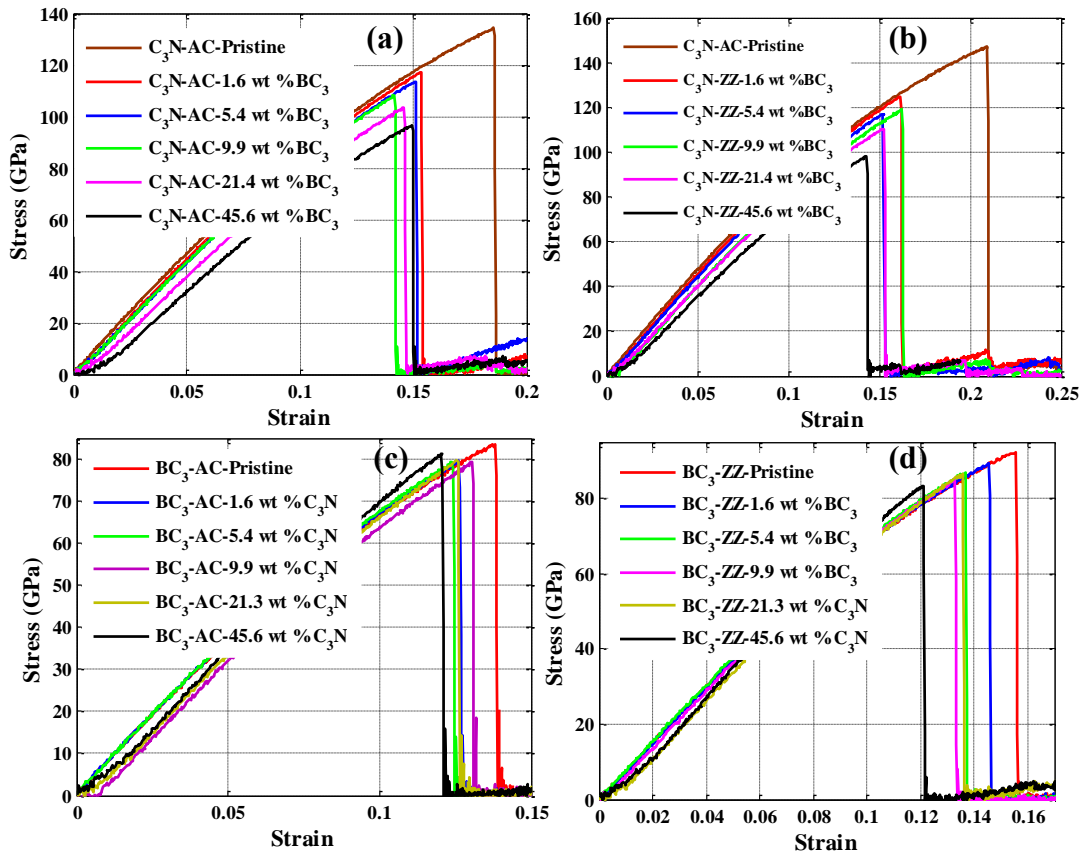


Figure 7. Stress-strain curve of BC₃ sheet embedded into the C₃N in both armchairs (a) and zigzag (b), and C₃N sheet embedded into the BC₃ in both armchair (c) and zigzag (d).

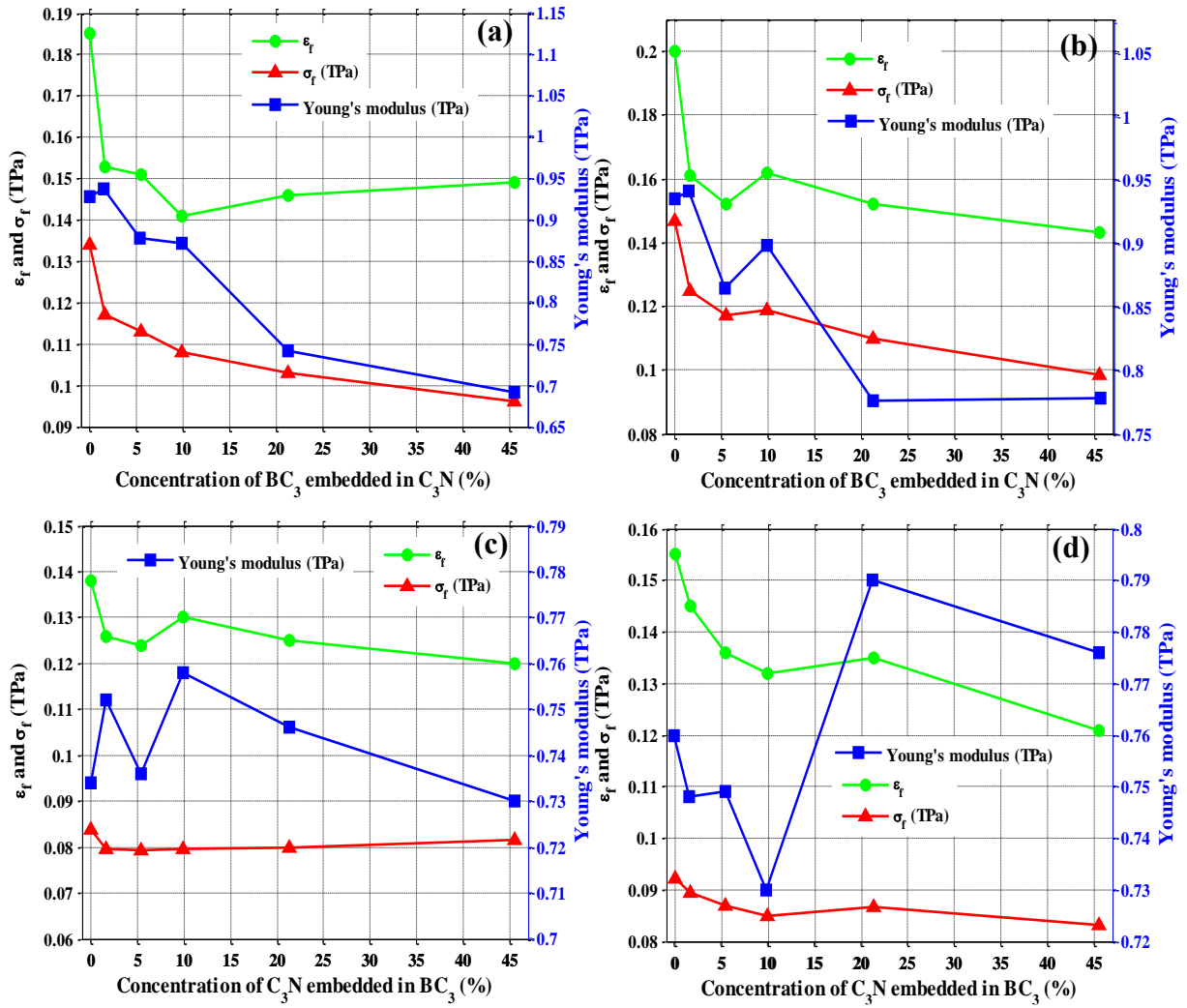


Figure 8. The dependence of Young's modulus, failure strength, and failure strain on the concentration of BC_3 sheet embedded in C_3N in both armchairs (a) and zigzag (b) directions and concentration of C_3N sheet embedded in the BC_3 in both armchair (c) and zigzag (d).

Table 2. Comparison of Young's modulus, failure strength and strain of concentration of BC_3 sheet embedded in C_3N . Concentration of C_3N sheet embedded in the BC_3 in both AC and ZZ direction with different weight percentages and modes using molecular dynamics simulations.

Structure		Failure Stress (GPa)				Failure Strain (%)				Young's modulus (GPa)			
		Value (GPa)		Variation (%)		Value (%)		Variation (%)		Value (GPa)		Variation (%)	
		AC	ZZ	AC	ZZ	AC	ZZ	AC	ZZ	AC	ZZ	AC	ZZ
Concentration of BC_3 embedded in C_3N (%)	0	134	147	-	-	18.5	20	-	-	928	936	-	-
	1.6	117	125	-13	-15	15.3	16.1	-17	-20	936	942	+0.8	-0.6
	5.4	113	117	-16	-20	15.1	15.2	-18	-24	878	865	-5.3	-7.5
	9.9	108	119	-19	-19	14.1	16.2	-12	-19	871	899	-6.1	-3.9

	21.3	104	110	-22	-25	14.6	15.2	-18	-24	741	776	-20	-17
	45.6	97	98	-28	-33	14.9	14.3	-23	-29	691	778	-26	-17
Concentration of C₃N embedded in BC₃ (%)	0	83.7	92.2	-	-	13.8	15.5	-	-	734	760	-	-
	1.6	79.5	89.4	-5	-3	12.6	14.5	-8.7	-6.4	752	748	+2.4	-1.5
	5.4	79.3	87	-5.2	-5.6	12.4	13.6	-10	-12	736	749	+0.2	-1.4
	9.9	79.5	85	-5	-7.8	13	13.2	-5.8	-15	758	730	+3.2	-3.9
	21.3	79.8	86.6	-4.6	-6	12.5	13.5	-9.4	-13	746	790	+1.6	+3.9
	45.6	81.5	83.2	-2.6	-9.7	12	12.1	-13	-22	730	776	-0.5	+2.1

To better understand the failure behavior and to observe the stress distribution in this part of the work, the von Mises stress for two similar states of weight percentage (9.9% in AC direction) is shown in Figure 9. Stress distribution in both hybrid structures must be regarded. The better performance of C₃N in stress distribution is apparent, so failure occurs in BC₃, and strong C-N bonds prevent rupture of the C₃N area. The results also illustrate that although there are maximum stresses in the C₃N regions, the C₃N structure is more resistant. As the strain increases, these maximum stresses transferred to the interface between the two structures and failure occurs in the BC₃ regions. Various mechanisms also govern these behaviors in nanoscale. For example, factors such as atomic lattice, edge structure, the concentration of defect, ripples, and out-of-plane and residual strains in the structure affect fracture behavior and other properties of 2D materials [48 ,47].

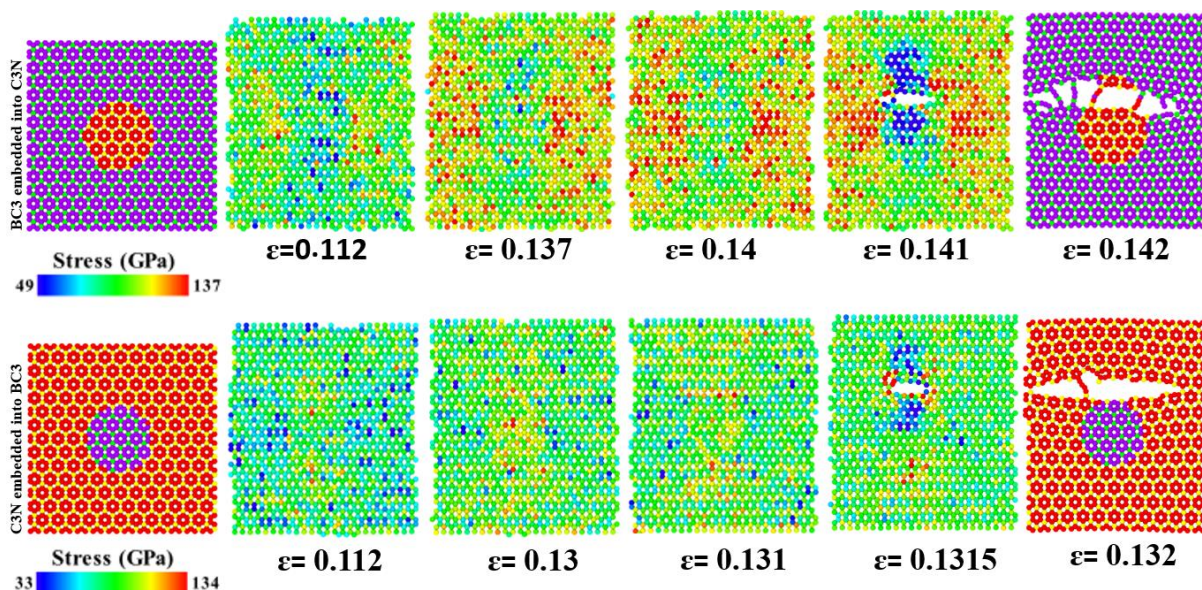


Figure 9. Von Mises stress distribution for hybrid structures of C₃N/BC₃ with wt. %9.9 concentration.

The mechanism of graphene failure is influenced by the lattice structure, which includes a fracture path, and alternately changes the rotation and rupture of the bonds. The shape of the edges and the concentration of defects in the two-dimensional material can change the failure modes from brittle to flexible under tensile loads. Graphene exhibits brittle behavior under tensile loads, however, when it is combined with other two-dimensional materials, it shows a stable plastic behavior. For instance, when the concentration of the defects in graphene increases, the graphene exhibits ductile behavior. This behavior has been observed in other 2D materials as well. In phosphorene, the stress distribution is almost uniform, except in the presence of defects, when the stress is concentrated around these defects. But here the two pure and hybrid structures of C_3N and BC_3 have brittle behavior which, in this case, did not act similarly to the graphene and did not show a new mechanical behavior.

3.4 The effect of strain rate and defect

In this section, the effect of strain rate and the presence of defects in the hybrid structure were investigated. Regarding figure 5, the effect of strain rate on the stress-strain curve is negligible, and, therefore ignored. On the other hand, in two-dimensional materials, various types of defects can interact in the structure constructively or destructively. Their effects on material failure behavior would, therefore, be different[49]. In 2-D materials, mechanical properties are generally sensitive to defects and failure behaviors in these materials are evident[50]. Since the various types of defects at the interface of C_3N and BC_3 are likely to happen, in this study, different types of defects were considered such as single vacancy and double vacancy for BC_3 embedded in C_3N at a concentration of 9.9%.

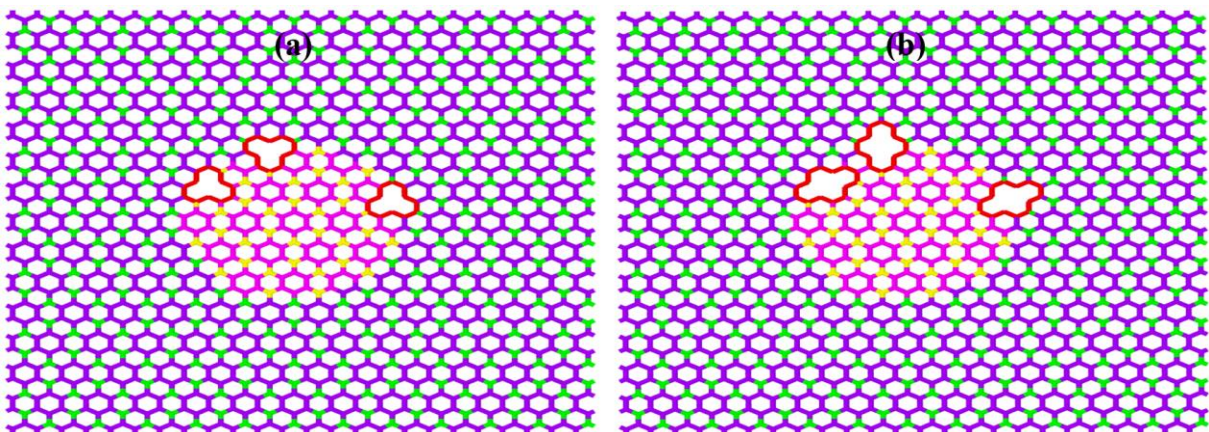


Figure 10. The initial configuration of the hybrid nanosheets (C_3N -AC-9.9 wt % BC_3) containing (a) single vacancies , (b) divacancies at the interface. The purple, green, pink, and yellow bonds represent the carbon atoms (in C_3N), nitrogen, carbon (in BC_3), and boron, respectively. Here, the defect area is shown with red bonds.

Figure 10 demonstrates the variations of mechanical characteristics in the presence of vacancy defects. The results show that by increasing the number of single defects at the intersection of system, the stress, failure strain, and Young's modulus reduced by 20, 30, and 50%, respectively. While embedding the double defects at the intersection reduces the stress, failure strain, and Young's modulus by 60, 40, and 60% , respectively. It is clear that the effect of the DV fault is greater and will cause a system failure. However, the presence of a vacancy defect does not always reduce the mechanical properties and in some cases may lead to the removal of atoms in the structure where the stress concentration was high, so the result can be reversed. It should be noted that Griffith's theory cannot be used to describe the mechanics of failure criteria because this theory does not take into account factors in the nanostructure, such as atomic lattice, defective concentration, and inherent residual strain. Structural mechanics, on the other hand, predict failure in 2D materials by analyzing bond deformation, which depends on the length and angle of the bond. Therefore, the study of mechanical properties in such materials can be concluded based on the maximum criterion of bond tension.

Unlike C₃N and BC₃, which were flawless, the main source of cracking in such structures was the rupture of bonds in the vicinity of vacancy. As a result, the possibility of creating nanopores around broken bonds increased. At low concentrations of vacancy, the corresponding 2D materials, such as graphene, exhibited brittle behavior under tensile loads, whereas when these concentrations increase, they exhibited ductile behavior. In other 2D materials, this behavior has been observed so that the stress distribution in phosphorene is almost uniform, except in cases where in the presence of a defect, the compensating stress will be concentrated around these defects. Stress concentrations caused broken bonds to form in defective areas during the deformation process. We observed that the presence of vacancy and fracture of the bond lead to the creation of gaps around it and perpendicular to the direction of tension, ultimately leading to the spontaneous failure of the structure. It should be emphasized that the reduction of mechanical properties also depends on the load and the type of defect.

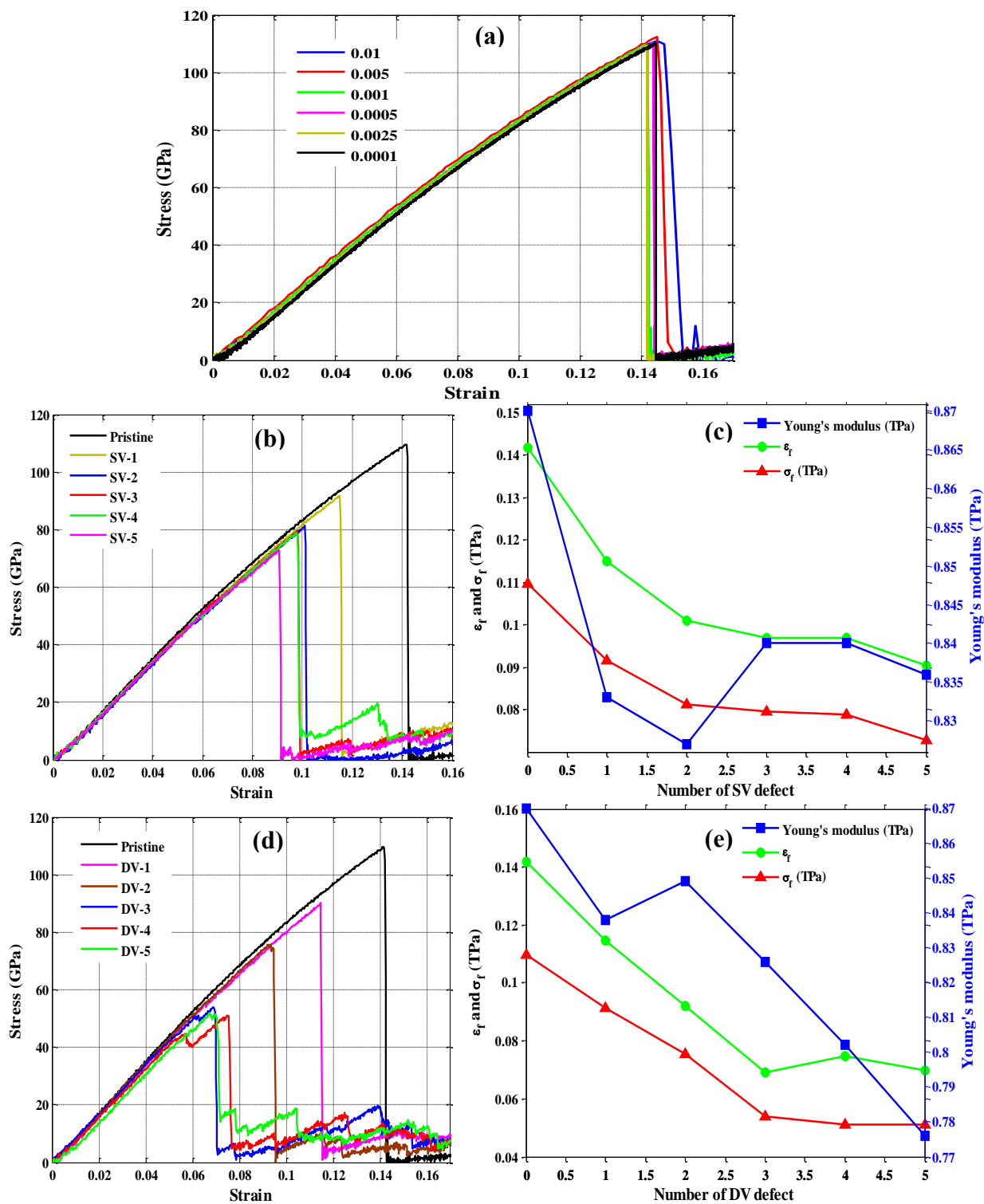


Figure 11. (a),(b) and (d) The Stress–strain curve of hybrid system (BC3 embedded in C3N with wt. %9.9 concentration) with different strain rate (0.01 to 0.0001 ps⁻¹) and in the presence of SV and DV, respectively. The Young's modulus, fracture strength, and strain are shown by increasing the number of defects for SV (c) and DV (e).

4 Conclusions

This study investigated the mechanical properties of the C_3N and BC_3 single-layer doped with atoms of boron and nitrogen by using molecular dynamics simulation techniques. It demonstrated that by adding 5% of boron atom to the C_3N structure in the armchair direction, Young's modulus, failure stress, and strain reduce by 6, 19, and 20 percent, respectively. And, when we added nitrogen atom to the BC_3 structure, failure stress and strain reduced by 1.5 and 2%, respectively, but Young's modulus increased by 1%. The hybrid of these two nanosheets were studied and it was revealed that monolayer C_3N increases the mechanical properties of BC_3 due to strong bonds between C-N, but adding BC_3 to C_3N significantly reduces the mechanical properties of C_3N . The results show that the combined structure of C_3N - 9.9 wt. % BC_3 in the AC direction are associated with a decrease of 6, 20, and 24 percent for Young's modulus, failure stress, and strain. While in the hybrid structure of BC_3 - 9.9 wt. % C_3N in the AC direction, fracture stress and strain decreased by 5 and 6 percent Young's modulus increased by 4 percent. Moreover, we analyzed the von Mises stress distribution behavior to create two-dimensional nanoparticles composed of C_3N and BC_3 . The C_3N structure has a better stress distribution than BC_3 . The findings show the outstanding mechanical properties of BC_3 and C_3N , which can introduce them as new catalysts for designing new nanoelectronics and nanoelectromechanical devices.

Acknowledgment

The author, Fatemeh Molaei, wishes to express her thanks for the financial support of Freeport McMoRan Inc. in her education.

5 References

- [1] A. H. Castro Neto, F. Guinea, N. M. R. Peres, K. S. Novoselov, and A. K. Geim, "The electronic properties of graphene," *Reviews of Modern Physics*, vol. 81, no. 1, pp. 109-162, 01/14/ 2009, doi: 10.1103/RevModPhys.81.109.
- [2] A. K. Geim and K. S. Novoselov, "The rise of graphene," in *Nanoscience and Technology*: Co-Published with Macmillan Publishers Ltd, UK, 2009, pp. 11-19.
- [3] K. S. Novoselov *et al.*, "Electric Field Effect in Atomically Thin Carbon Films," *Science*, vol. 306, no. 5696, pp. 666-669, October 22, 2004 2004, doi: 10.1126/science.1102896.
- [4] D. Ghosh, P. Parida, and S. K. Pati, "Line defects at the heterojunction of hybrid boron nitride-graphene nanoribbons," *Journal of Materials Chemistry C*, 10.1039/C3TC31784F vol. 2, no. 2, pp. 392-398, 2014, doi: 10.1039/C3TC31784F.
- [5] K. E. Eshkalak, S. Sadeghzadeh, and M. Jalaly, "Mechanical properties of defective hybrid graphene-boron nitride nanosheets: A molecular dynamics study," *Computational Materials Science*, vol. 149, pp. 170-181, 2018.
- [6] K. Einalipour Eshkalak, S. Sadeghzadeh, and M. Jalaly, "The mechanical design of hybrid graphene/boron nitride nanotransistors: Geometry and interface effects," *Solid State Commun.*, vol. 270, pp. 82-86, 2018/02/01/ 2018, doi: <https://doi.org/10.1016/j.ssc.2017.12.001>.
- [7] Y. Mao *et al.*, "Lithium storage in nitrogen-rich mesoporous carbon materials," *Energy & Environmental Science*, 10.1039/C2EE21817H vol. 5, no. 7, pp. 7950-7955, 2012, doi: 10.1039/C2EE21817H.
- [8] L. S. Panchakarla *et al.*, "Synthesis, Structure, and Properties of Boron- and Nitrogen-Doped Graphene," *Advanced Materials*, vol. 21, no. 46, pp. 4726-4730, 2009/12/11 2009, doi: 10.1002/adma.200901285.
- [9] Z.-S. Wu, W. Ren, L. Xu, F. Li, and H.-M. Cheng, "Doped Graphene Sheets As Anode Materials with Superhigh Rate and Large Capacity for Lithium Ion Batteries," *ACS Nano*, vol. 5, no. 7, pp. 5463-5471, 2011/07/26 2011, doi: 10.1021/nn2006249.
- [10] S. Feng, Z. Lin, X. Gan, R. Lv, and M. Terrones, "Doping two-dimensional materials: ultra-sensitive sensors, band gap tuning and ferromagnetic monolayers," *Nanoscale Horizons*, 10.1039/C6NH00192K vol. 2, no. 2, pp. 72-80, 2017, doi: 10.1039/C6NH00192K.
- [11] Y. Siwei *et al.*, "C3N—A 2D Crystalline, Hole-Free, Tunable-Narrow-Bandgap Semiconductor with Ferromagnetic Properties," *Advanced Materials*, vol. 29, no. 16, p. 1605625, 2017, doi: doi:10.1002/adma.201605625.
- [12] H. Tanaka *et al.*, "Novel macroscopic BC3 honeycomb sheet," *Solid State Communications*, vol. 136, no. 1, pp. 22-25, 2005/10/01/ 2005, doi: <https://doi.org/10.1016/j.ssc.2005.06.025>.
- [13] Y. Qie, J. Liu, S. Wang, S. Gong, and Q. Sun, "C3B monolayer as an anchoring material for lithium-sulfur batteries," *Carbon*, vol. 129, pp. 38-44, 2018/04/01/ 2018, doi: <https://doi.org/10.1016/j.carbon.2017.11.068>.

- [14] P. Bhauriyal, A. Mahata, and B. Pathak, "Graphene-like Carbon–Nitride Monolayer: A Potential Anode Material for Na- and K-Ion Batteries," *The Journal of Physical Chemistry C*, vol. 122, no. 5, pp. 2481-2489, 2018/02/08 2018, doi: 10.1021/acs.jpcc.7b09433.
- [15] E. Chigo-Anota, M. A. Alejandro, A. B. Hernández, J. J. S. Torres, and M. Castro, "Long range corrected-wPBE based analysis of the H₂O adsorption on magnetic BC₃ nanosheets," *RSC Advances*, 10.1039/C5RA27231A vol. 6, no. 24, pp. 20409-20421, 2016, doi: 10.1039/C5RA27231A.
- [16] H. Zhang, Y. Liao, G. Yang, and X. Zhou, "Theoretical Studies on the Electronic and Optical Properties of Honeycomb BC₃ monolayer: A Promising Candidate for Metal-free Photocatalysts," *ACS Omega*, vol. 3, no. 9, pp. 10517-10525, 2018/09/30 2018, doi: 10.1021/acsomega.8b01998.
- [17] Y. Tang, M. Zhang, Z. Shen, J. Zhou, H. Chai, and X. Dai, "Non-metal atom anchored BC₃ sheet: a promising low-cost and high-activity catalyst for CO oxidation," *New Journal of Chemistry*, 10.1039/C7NJ04877G vol. 42, no. 5, pp. 3770-3780, 2018, doi: 10.1039/C7NJ04877G.
- [18] B. Mortazavi, M. Shahrokhi, M. Raeisi, X. Zhuang, L. F. C. Pereira, and T. Rabczuk, "Outstanding strength, optical characteristics and thermal conductivity of graphene-like BC₃ and BC₆N semiconductors," *Carbon*, vol. 149, pp. 733-742, 2019/08/01/ 2019, doi: <https://doi.org/10.1016/j.carbon.2019.04.084>.
- [19] Y. Tang, M. Zhang, W. Chen, X. Cui, Y. Li, and X. Dai, "Structural, electronic, and magnetic properties of gas molecules on Mo-, Si-, and Pt-doped BC₃ sheets," *Journal of Physics and Chemistry of Solids*, vol. 121, pp. 247-255, 2018/10/01/ 2018, doi: <https://doi.org/10.1016/j.jpcc.2018.05.037>.
- [20] M. D. Esrafil and S. Heydari, "B-doped C₃N monolayer: a robust catalyst for oxidation of carbon monoxide," *Theoretical Chemistry Accounts*, vol. 138, no. 4, p. 57, 2019/04/13 2019, doi: 10.1007/s00214-019-2444-z.
- [21] H. Cui, C. Yan, P. Jia, and W. Cao, "Adsorption and sensing behaviors of SF₆ decomposed species on Ni-doped C₃N monolayer: A first-principles study," *Applied Surface Science*, vol. 512, p. 145759, 2020/05/15/ 2020, doi: <https://doi.org/10.1016/j.apsusc.2020.145759>.
- [22] H. Tafrishi, S. Sadeghzadeh, R. Ahmadi, F. Molaei, F. Yousefi, and H. Hassanloo, "Investigation of tetracosane thermal transport in presence of graphene and carbon nanotube fillers—A molecular dynamics study," *Journal of Energy Storage*, vol. 29, p. 101321, 2020/06/01/ 2020, doi: <https://doi.org/10.1016/j.est.2020.101321>.
- [23] J. Beheshtian, A. A. Peyghan, and M. Noei, "Sensing behavior of Al and Si doped BC₃ graphenes to formaldehyde," *Sensors and Actuators B: Chemical*, vol. 181, pp. 829-834, 2013/05/01/ 2013, doi: <https://doi.org/10.1016/j.snb.2013.02.086>.
- [24] Z. Yang and J. Ni, "Li-doped BC₃ sheet for high-capacity hydrogen storage," *Applied Physics Letters*, vol. 100, no. 18, p. 183109, 2012/04/30 2012, doi: 10.1063/1.4711038.
- [25] B. He, J. Shen, D. Ma, Z. Lu, and Z. Yang, "Boron-Doped C₃N Monolayer as a Promising Metal-Free Oxygen Reduction Reaction Catalyst: A Theoretical Insight," *The Journal of Physical Chemistry C*, vol. 122, no. 35, pp. 20312-20322, 2018/09/06 2018, doi: 10.1021/acs.jpcc.8b05171.

- [26] Q. Wu *et al.*, "In situ chemical vapor deposition of graphene and hexagonal boron nitride heterostructures," *Current Applied Physics*, vol. 16, no. 9, pp. 1175-1191, 2016/09/01/ 2016, doi: <https://doi.org/10.1016/j.cap.2016.04.024>.
- [27] A. A. Tedstone *et al.*, "Mechanical Properties of Molybdenum Disulfide and the Effect of Doping: An in Situ TEM Study," *ACS Applied Materials & Interfaces*, vol. 7, no. 37, pp. 20829-20834, 2015/09/23 2015, doi: 10.1021/acsami.5b06055.
- [28] Y. Ganesan *et al.*, "Effect of Nitrogen Doping on the Mechanical Properties of Carbon Nanotubes," *ACS Nano*, vol. 4, no. 12, pp. 7637-7643, 2010/12/28 2010, doi: 10.1021/nn102372w.
- [29] M. Izadifar, R. Abadi, A. N. Jam, and T. Rabczuk, "Investigation into the effect of doping of boron and nitrogen atoms in the mechanical properties of single-layer polycrystalline graphene," *Computational Materials Science*, vol. 138, pp. 435-447, 2017/10/01/ 2017, doi: <https://doi.org/10.1016/j.commatsci.2017.06.038>.
- [30] O. Akbari, R. Ansari, and S. Rouhi, "Mechanical properties of pristine and Fe, V and Ti doped arsenene: density functional theory calculation," *Materials Research Express*, vol. 5, no. 1, p. 015025, 2018/01/08 2018, doi: 10.1088/2053-1591/aaa217.
- [31] K. Einalipour Eshkalak, S. Sadeghzadeh, and F. Molaei, "Interfacial Thermal Resistance Mechanism for the Polyaniline (C3N)–Graphene Heterostructure," *The Journal of Physical Chemistry C*, vol. 124, no. 26, pp. 14316-14326, 2020/07/02 2020, doi: 10.1021/acs.jpcc.0c02051.
- [32] B. Mortazavi, S. Ahzi, V. Toniazzo, and Y. Rémond, "Nitrogen doping and vacancy effects on the mechanical properties of graphene: A molecular dynamics study," *Physics Letters A*, vol. 376, no. 12, pp. 1146-1153, 2012/02/27/ 2012, doi: <https://doi.org/10.1016/j.physleta.2011.11.034>.
- [33] B. Mortazavi and S. Ahzi, "Molecular dynamics study on the thermal conductivity and mechanical properties of boron doped graphene," *Solid State Communications*, vol. 152, no. 15, pp. 1503-1507, 2012/08/01/ 2012, doi: <https://doi.org/10.1016/j.ssc.2012.04.048>.
- [34] S. Sadeghzadeh, "Effects of vacancies and divacancies on the failure of C3N nanosheets," *Diamond Relat. Mater.*, vol. 89, pp. 257-265, 2018/10/01/ 2018, doi: <https://doi.org/10.1016/j.diamond.2018.09.018>.
- [35] B. Mortazavi, "Ultra high stiffness and thermal conductivity of graphene like C3N," *Carbon*, vol. 118, pp. 25-34, 2017/07/01/ 2017, doi: <https://doi.org/10.1016/j.carbon.2017.03.029>.
- [36] A. H. N. Shirazi, R. Abadi, M. Izadifar, N. Alajlan, and T. Rabczuk, "Mechanical responses of pristine and defective C3N nanosheets studied by molecular dynamics simulations," *Computational Materials Science*, vol. 147, pp. 316-321, 2018/05/01/ 2018, doi: <https://doi.org/10.1016/j.commatsci.2018.01.058>.
- [37] R. K. Zahedi, A. H. N. Shirazi, P. Alimouri, N. Alajlan, and T. Rabczuk, "Mechanical properties of graphene-like BC3; a molecular dynamics study," *Computational Materials Science*, vol. 168, pp. 1-10, 2019/10/01/ 2019, doi: <https://doi.org/10.1016/j.commatsci.2019.05.053>.
- [38] S. Zhao and J. Xue, "Mechanical properties of hybrid graphene and hexagonal boron nitride sheets as revealed by molecular dynamic simulations," *Journal of Physics D: Applied Physics*, vol. 46, no. 13, p. 135303, 2013/03/05 2013, doi: 10.1088/0022-3727/46/13/135303.

- [39] N. Ding, X. Chen, and C.-M. L. Wu, "Mechanical properties and failure behaviors of the interface of hybrid graphene/hexagonal boron nitride sheets," *Scientific Reports*, Article vol. 6, p. 31499, 08/16/online 2016, doi: 10.1038/srep31499
- <https://www.nature.com/articles/srep31499#supplementary-information>.
- [40] S. Plimpton, "Fast parallel algorithms for short-range molecular dynamics," United States, 1993-05-01 1993. [Online]. Available: <https://www.osti.gov/servlets/purl/10176421>
- [41] A. Stukowski, "Visualization and analysis of atomistic simulation data with OVITO—the Open Visualization Tool," *Modelling and Simulation in Materials Science and Engineering*, vol. 18, no. 1, p. 015012, 2009/12/15 2009, doi: 10.1088/0965-0393/18/1/015012.
- [42] A. Kınacı, J. B. Haskins, C. Sevik, and T. Çağın, "Thermal conductivity of BN-C nanostructures," *Physical Review B*, vol. 86, no. 11, p. 115410, 09/06/ 2012, doi: 10.1103/PhysRevB.86.115410.
- [43] L. Lindsay and D. A. Broido, "Optimized Tersoff and Brenner empirical potential parameters for lattice dynamics and phonon thermal transport in carbon nanotubes and graphene," *Physical Review B*, vol. 81, no. 20, p. 205441, 05/27/ 2010, doi: 10.1103/PhysRevB.81.205441.
- [44] K. E. Eshkalak, S. Sadeghzadeh, and M. Jalaly, "Studying the effects of longitudinal and transverse defects on the failure of hybrid graphene-boron nitride sheets: A molecular dynamics simulation," *Physica E: Low-dimensional Systems and Nanostructures*, vol. 104, pp. 71-81, 2018.
- [45] Y.-Y. Zhang, Q.-X. Pei, Z.-D. Sha, and Y.-W. Zhang, "A molecular dynamics study of the mechanical properties of h-BCN monolayer using a modified Tersoff interatomic potential," *Physics Letters A*, vol. 383, no. 23, pp. 2821-2827, 2019/08/12/ 2019, doi: <https://doi.org/10.1016/j.physleta.2019.05.055>.
- [46] Y. Gong *et al.*, "Direct chemical conversion of graphene to boron- and nitrogen- and carbon-containing atomic layers," *Nature Communications*, vol. 5, no. 1, p. 3193, 2014/01/24 2014, doi: 10.1038/ncomms4193.
- [47] K. E. Eshkalak, S. Sadeghzadeh, and M. Jalaly, "Thermal resistance analysis of hybrid graphene-boron nitride nanosheets: The effect of geometry, temperature, size, strain and structural defects," *Computational Materials Science*, vol. 174, p. 109484, 2020/03/01/ 2020, doi: <https://doi.org/10.1016/j.commatsci.2019.109484>.
- [48] H. Qin, V. Sorkin, Q.-X. Pei, Y. Liu, and Y.-W. Zhang, "Failure in Two-Dimensional Materials: Defect Sensitivity and Failure Criteria," *Journal of Applied Mechanics*, vol. 87, no. 3, 2020, doi: 10.1115/1.4045005.
- [49] K. E. Eshkalak, S. Sadeghzadeh, and F. Molaei, "Aluminum nanocomposites reinforced with monolayer polyaniline (C3N): assessing the mechanical and ballistic properties," *RSC Advances*, 10.1039/D0RA03204B vol. 10, no. 33, pp. 19134-19148, 2020, doi: 10.1039/D0RA03204B.
- [50] H. Tafriahi, S. Sadeghzadeh, F. Molaei, and H. Siavoshi, "Investigating the effects of adding hybrid nanoparticles, graphene and boron nitride nanosheets, to octadecane on its thermal properties," *RSC Advances*, 10.1039/D0RA01847C vol. 10, no. 25, pp. 14785-14793, 2020, doi: 10.1039/D0RA01847C.

6 Data Availability

Derived data supporting the findings of this study are available from the corresponding author Dr. S. S. on request.